Cell. Mol. Life Sci. (2013) 70:711–728
DOI 10.1007/s00018-012-1157-4

Cellular and Molecular Life Sciences

RESEARCH ARTICLE

MBD6 is a direct target of Oct4 and controls the stemness and differentiation of adipose tissue-derived stem cells

Jin Sun Jung · Min Ki Jee · Hyun Tae Cho · Jee In Choi · Young Bin Im · Oh Hyun Kwon · Soo Kyung Kang

Received: 18 May 2012 / Revised: 29 August 2012 / Accepted: 30 August 2012 / Published online: 30 September 2012

Abstract Argonaute 2 (Ago2) is a pivotal regulator of cell fate in adult stem cells. Its expression is significantly downregulated in late passages of cells, concomitant with a prominent increase in Ago2 cytosolic localization in single cells. Nuclear localization of Ago2 is crucial for the survival, proliferation, and differentiation of hATSCs (human adipose tissue-derived stem cells), mediated by the specific binding of the regulatory regions of functional genes, which positively or negatively altered gene expression. Ago2 targets genes that control stemness, reactive oxygen species scavenging, and microRNA expression, all of which are crucial for hATSC survival and self-renewal. Ago2 promotes cell proliferation and self-renewal by activating the expression of octamer-binding transcription factor 4 (Oct4). We confirmed the direct regulation of Oct4 activity by Ago2, as indicated by the results of the ChIP analysis. Methyl-CpG-binding protein 6 (MBD6) was detected as an Oct4 regulatory gene. As predicted, knockdown of MBD6 expression attenuated cell proliferation and eventually induced cell death. We hypothesized that MBD6 functions downstream of Oct4 in the regulation of stemness-related genes, cell proliferation, self-renewal activity, and survival. MBD6 also promoted cell transdifferentiation into neural and endodermal β-cells while significantly attenuating differentiation into the mesodermal lineage. We demonstrate that MBD6 is regulated by Ago2 via an interaction with Oct4, which alters self-renewal and gene expression in hATSCs. MBD6 was promoted cell proliferation through a novel set of signal mediators that may influence differentiation by repressing MBD2 and MBD3, which are possibly recruited by germ cell nuclear factor (GCNF).

Keywords Ago2 · hATSC · Methyl-CpG-binding protein 6 · Oct4

Abbreviations

Ago2	Argonaute2
BRCA2	Breast cancer type 2 susceptibility protein
BrdU	5-bromo-2′-deoxyuridine
CDK	Cyclin-dependent kinases
CFU	Colony forming unit
CM-Dil	Chloromethyl-benzamidodialkylcarbocyanine
DCAF-DA	1′, 7′-Dichlodihydrofluorescein diacetate
FOXG1	Forkhead box protein G1
GFAP	Glial fibrillary acidic protein
hATSC	human Adipose Tissue-derived Stem Cell
JNK	c-Jun N-terminal kinases
KLF4	Krueppel-like factor 4
MAP2	Microtubule-associated protein 2
MBD	Methyl-CpG-binding protein
NF160	Neurofilament 160
Oct4	Octamer-binding transcription factor 4
PPARγ	Peroxisome proliferator-activated receptor gamma
RISC	RNA-induced silencing complex
ROS	Reactive Oxygen Species

Jin Sun Jung and Min Ki Jee contributed equally to this work.

Electronic supplementary material The online version of this article (doi:10.1007/s00018-012-1157-4) contains supplementary material, which is available to authorized users.

J. S. Jung · M. K. Jee · H. T. Cho · J. I. Choi · Y. B. Im · O. H. Kwon · S. K. Kang (✉)
Laboratory of Stem Cell Biology, Department of Biotechnology, College of Veterinary Medicine, Seoul National University, Seoul 151-742, Republic of Korea
e-mail: sookang@snu.ac.kr

Runx3	Runt-related transcription factor 3
SEPN1	Selenoprotein N1
Sox2	SRY (sex determing region Y)-box 2
STAT3	Signal transducer and activator of transcription 3
Tuj	beta III tubulin
USP44	Upiquitin carboxyl-terminal hydrolase 44

Introduction

Argonaute (Ago) proteins have specific posttranscriptional functions during microRNA (miRNA) processing that enhance the production and/or stability of mature miRNAs. Murchison et al. [1] found that Dicer-null cells have significantly higher levels of pre-miRNAs associated with endogenous Ago2. Immunofluorescence studies revealed the presence of nuclear and cytoplasmic Ago2 in HeLa cells, consistent with previous results demonstrating Ago2 localization in human cell nuclei and RNA-induced silencing complex (RISC) activity in mammalian cell nuclear extracts [2, 3]. Collectively, these findings indicate the presence of active Ago2/miRNA complexes in the nucleus. Additionally, Ago2-deficient mice have several developmental abnormalities that begin approximately halfway through gestation. Prenatal embryos have been found to exhibit phenotypes such as neural tube closure defects and forebrain developmental abnormalities [4]. Among the four Ago subunits, Ago2 is thought to be required during development. Transfection of full-length Ago2 enhances proliferation, reduces cell–cell adhesion and increases migration in breast cancer cells. In this context, Ago2 is regulated at the transcriptional and post-translational levels, implicating Ago2-induced miRNA activity in tumorigenesis [5]. We previously developed a cell-based system with hATSCs (human adipose tissue-derived stem cells) with the potential to differentiate into multiple cell lineages, including neurons [6, 7], and showed that adult somatic stem cells have the capacity to contribute to the regeneration of various tissues. These findings suggest that the restriction of differentiation is not completely irreversible and can be reprogrammed by dedifferentiation and transdifferentiation processes. In our system, as cells age, telomeres are gradually shortened due to insufficient recovery of telomere lengths, and mitochondrial deficiencies occur because of accumulating mutations [8–10]. However, because aging is a complex process, it cannot be sufficiently explained by these two theories. In our previous study, we reported that Ago2 is a novel candidate for regulating the aging of hATSCs [11] and, based on our results, we suggested that Ago2 has dual functions. First, Ago2 participates in cytosolic RNA-induced silencing complexes [12]. Second, Ago2 operates as a transcription factor in the nucleus. Ago2 directly inhibits the expression of miR10b and SEPN1, which inhibit reactive oxygen species (ROS) scavenging [11]. To define Ago2 regulatory mechanisms, we performed chromatin immunoprecipitation (ChIP-PCR) to assess genomic binding affinity and extracted the DNA fragments that were regulatory regions bound by Ago2. We found that Ago2 was bound to the Oct4 promoter region. Oct4 (octamer-binding transcription factor 4) is a crucial transcription factor that sustains self-renewal activity and differentiation of adult stem cells, including hATSCs. Moreover, Oct4 is one of four factors (Oct4, Sox2, Nanog, c-Myc, or Lin28) that promote somatic cell reprogramming into induced pluripotent stem cells [13, 14]. As a critical regulator of stem cell pluripotency, Oct4 is highly expressed in the early stages of the mammalian embryo and in the inner cell mass of the blastocyst. Downregulation of Oct4 expression during trophoblast differentiation, the generation of mutant embryos, and conversion into exclusively trophoblast-like cells following Oct4 knockout revealed that Oct4 was required to either establish or maintain pluripotency in the developing embryo. Although the mechanisms of Oct4 in the regulation of cell fate in embryonic stem (ES) cells have been widely investigated, the role of Oct4 in the postnatal stage is still unclear. Our previous study also showed that Oct4 is associated with the undifferentiated pluripotent state of stem cell populations derived from various adult tissues. To clarify the function of Oct4 in adult cells, we investigated the regulation of the expression of Oct4 and other embryonic genes in fully differentiated cells and discovered that Oct4 is also expressed at the gene and protein levels in hATSCs [9].

In contrast, methyl-CpG-binding proteins (MeCPs) are involved in methylation-dependent gene repression and affect chromatin structure [15–18]. The MeCP1 complex and MeCP2 were initially reported to specifically bind to methylated DNAs [6, 19] and repress transcription by recruiting histone deacetylases and corepressor proteins [20–22]. An additional four MeCP members, methyl-CpG binding domain 1 (MBD1), MBD2, MBD3, and MBD4 (also known as MED1) have been identified based on their amino acid sequence homology to the MBD of MeCP2 [23, 24]. Five mammalian MeCP family proteins have been identified: MBD1, MBD2, MBD3, MBD4, and MeCP2 [4]. These proteins bind to DNA as a monomer, independent of the sequence context outside of the CpG sequence [25, 26]. MBD1 and MBD2 proteins bind to methylated DNA and recruit different histone deacetylase (HDAC)- and histone methyltransferase (HMT)-containing complexes that control chromatin compaction and gene silencing. MBDs play important roles in methylation-mediated transcriptional silencing: MBD1 interacts with other cellular factors and forms specific complexes via either CXXC domains or the

C terminus; MeCP2, MBD2, and MBD3 are embedded in histone deacetylase complexes and involved in packing genomic DNA into inactive chromatin, which leads transcriptional repression [20–22, 27, 28].

We recently found that MBD6 overexpression triggers Oct4 activity, which enhances stemness, REST, CDKs, and RUNX3 expression while upregulating Ago2 expression. In contrast, any interference in MBD6 expression effectively results in downregulation of stemness, REST, CDKs, RUNX3, and Ago2 expression and an improvement of cell proliferation in this context. MBD6 is one of the targets of Oct4 but it can also regulate Oct4. MBD6 expression significantly enhances cell proliferation and germ layer multi-differentiation.

Materials and methods

Isolation and culture of adipose tissue-derived stem cells

Human raw fat tissue obtained from patients' abdomens (following documented patient approval) was processed according to established methods to obtain stem cell vascular functions. To isolate the stem cells, the samples were digested with 0.075 % collagenase IV (Sigma, St. Louis, MO) and centrifuged at 1,200 *g* for 10 min to acquire a high-density cell pellet. The pellet was then suspended in red blood cell (RBC) lysis buffer (Biowhittaker, Walkersville, MD) and incubated for 10 min at room temperature to lyse the contaminating RBCs. The stem cell pellet was then collected and incubated overnight at 37 °C/5 % CO_2 in 10 % fetal bovine serum (FBS) containing α-MEM medium [Life Technologies (GibcoBRL). Rockville, MD]. This work was approved by the Seoul National University Institutional Review Board (IRB No. 0603/001-002), and the ethics committee specifically approved the procedure [7].

Cell viability and proliferation assay

Cell viability was assessed by visual cell counts in conjunction with trypan blue exclusion. Mitochondrial activity was assessed by measuring the ability of the cortical cultures to reduce 3,4,5-dimethyl thiazol-2-yl-2,5-diphenyl tetrazolium bromide (MTT; Sigma) to a colored formazan using a plate reader. In all viability assays, triplicate wells were established under each experimental condition, and each experiment was repeated at least three times. The raw data from each experiment were analyzed via analysis of variance (ANOVA) with Fisher's or *t* tests. For the flow cytometric analysis, cells were cultured in 100-mm dishes at densities that ensured exponential growth at the time of harvesting. Harvesting and processing protocols were used to detect DNA via flow cytometry with propidium iodide. The cells were analyzed with a BD Biosciences FACScan system (San Jose, CA). The percentages of cells in the G0/G1, S, and G2/M phases of the cell cycle were determined using a DNA histogram fitting program (MODFIT; Verity Software, Topsham, ME). A minimum of 10^4 events/samples was collected. Clonogenic cell growth experiments were conducted with control hATSCs and de-differentiated ATSCs for the detection of colony forming units (CFU). Cells were grown in culture media for 10–15 days, then fixed in methanol and stained with methylene blue. Colonies containing >50 cells were evaluated via light microscopy and scored as survivors. In each case, the number of colonies was counted according to the number of cells plated multiplied by the plating efficiency.

RT-PCR and primer sets

One week after the initiation of culturing, the total cellular RNA was extracted with Trizol (Life Technologies, Frederick, MA) from cultured hATSCs. Total RNA was reverse-transcribed into first-strand 7cDNA using an oligo-dT primer, then amplified via PCR using the indicated gene-specific primers (20 pM). The PCR reactions were conducted using an ABI 7700 Prism Sequence Detection System and SYBER green detection kit (Applied Biosystems, Foster, CA). The primer sequences were designed with Primer Express software (PE-Applied Biosystems, Warrington, UK) using gene sequences obtained from the GeneBank database (Supplementary Table S1).

Preparation of tissue whole extracts and western blot

For the confirmation of differentially expressed proteins following the de-ATSC, the cultured cells were pooled and lysed in 500 µl of lysis buffer (20 mM Tris–HCl, pH 7.5, 150 mM NaCl, 1 mM EDTA, 1 % Triton X-100, 2.5 mM sodium pyrophosphate, 1 mM EGTA, 1 mM glycerophosphate, 1 mM Na_3VO_4, and 1 mM PMSF). The lysates were clarified via 10 min of centrifugation at 15,000 *g*, and the total protein content was determined using a Bio-Rad Protein Assay kit (Hercules, CA). For western blotting, equal amounts (40 µg) of protein extracts in a lysis buffer were subjected to 10 % sodium dodecyl sulfate-polyacrylamide gel electrophoresis (SDS-PAGE) analysis and transferred to nitrocellulose membranes. Anti-MBD6 (1:1,000; Abcam, Cambridge, UK), anti-Rex1 (1:1,000; Abcam), anti-Nanog (1:1,000; Abcam), anti-BrdU (1:200; Abcam), anti-Histone H3 TrimethylK27 (1:1,000; Abcam), anti-Argonaute2 (1:1,000; Cell Signaling Technology, Beverly, MA), anti-GAPDH (1:1,000; Cell Signaling Technology), anti-P-SARK/JNK (1:1,000; Cell Signaling Technology), anti-p-P44/42 MARK (1:1000; Cell Signaling Technology), anti-β-catenin (1:1000; BD Biosciences), anti-Acetyl-Histone H3

(1:1,000; Cell Signaling Technology), anti-Histone H4 (1:1000; Cell Signaling Technology), anti-p-Akt (1:1000; Cell Signaling Technology), anti-p-P38/MARK (1:1,000; Cell Signaling Technology), anti-p-STAT3 (1:1000; Cell Signaling Technology), anti-PI3 K/P38 (1:1,000; Cell Signaling Technology), anti-p-c-Myc (1:1,000; Santa Cruz Biotechnolgy), anti-Oct4-3/4 (1:1,000; Santa Cruz Biotechnolgy), anti-Sox-2 (1:1,000; Santa Cruz Biotechnolgy), anti-Wnt-5a (1:1,000; Santa Cruz Biotechnolgy), anti-P53 (1:1,000; Santa Cruz Biotechnolgy), anti-P21 (1:1,000; Santa Cruz Biotechnolgy), anti-NF160 (1:40; Sigma), anti-dimethyl-Histone H3Lys4 (1:1,000; Millipore, Billerica, MA), anti-trimethyl- Histone H3Lys4 (1:1,000; Millipore), anti-GFAP (1:3,000; Dako, Carpinteria, CA), and anti-Tuj (1:500; BD Transduction, Franklin Lakes, NJ) antibodies were incubated with the membranes. The relative band intensities were determined using Quality-one 1-D Analysis software (Bio-Rad).

Small interfering RNA inhibition experiment

For the knockdown experiment, small intervering RNA (siRNA) duplexes against the functional genes, including Ago2, were synthesized. For transient transfection, cells about 60 % confluent were transfected with 10 μM siRNA using Lipofectamine (Invitrogen, Carlsbad, CA). The cells were harvested after 24 h for RNA isolation. Silencer Negative Control siRNA (Ambion Inc., Austin, TX) was utilized as a control for non-specific gene silencing. The siRNA transfection was conducted using DharmaFECT siRNA transfection reagents in accordance with the manufacturer's instructions (Dharmacon RNA Technologies, Lafayette, CO). Two complementary hairpin siRNA template oligonucleotides harboring 21-nt sequences of the target human genes were employed for transient transfection using 50 nM siRNA. Furthermore, the quantity of siRNA was optimized in accordance with the manufacturer's instructions. siRNAs for each gene (Silencer® predesigned siRNAs; Ambion) and scrambled siRNAs with the same nucleotide contents were assessed. When compared with unrelated control siRNAs and scrambled siRNAs, the gene-specific siRNAs resulted in an 80–90 % reduction in the mRNA levels of each gene, as determined by real-time PCR. The siRNA that provided the most efficient inhibition (90–95 %) was utilized for the experiments. We transfected the siRNAs for each gene into hATSCs and counted dye-excluding viable cells for 6 days to evaluate the presence of negative regulation of hATSC growth.

Bisulfite modification and sequencing of genomic DNA

Genomic DNA was purified via phenol/chloroform/isoamylalcohol extraction, followed by one chloroform extraction, after which the DNA was ethanol-precipitated. The DNA was then dissolved in distilled water. Bisulfite conversion was conducted using the EZ DNA Methylation–Gold kit (Zymo Research, Irvine, CA) as described by the manufacturer. Briefly, unmethylated cytosines in the DNA were converted into uracil via heat-denaturation of the DNA with a specially designed CT conversion reagent. The DNA was then desulfonated and subsequently cleaned and eluted. The bisulfite-modified DNA was then immediately utilized for PCR or stored at or below −20 °C. The converted DNA was amplified by the PCR or designed with MethPrimer (http://www.urogene.org/methprimer). The PCR reactions were conducted in a MyGenie 96 Gradient Thermal Block (Bioneer, Daejeon, South Korea) in accordance with the following protocol: 95 °C for 15 min, 40 cycles of 95 °C for 20 s, 43–58 °C for 40 s, and 72 °C for 30 s, followed by an extension at 72 °C for 10 min and soaking at 4 °C. The PCR products were cloned into bacteria (DH5α) with a pGEM T-Easy Vector System I (Promega, Madison, WI). The DNA extracted from the bacterial clones was analyzed via sequencing with the M13 reverse primer (5′-AGCGGATAACAATTTCACACAG GA-3′) using an ABI 3730XL capillary DNA sequencer (Applied Biosystems), and it is represented as rows of circles with each circle symbolizing the methylation state of one CpG.

ChIP analysis

To study of genome binding activity of Ago2, Oct4, MBD6, AcetylH3, AcetylH4, H3K4me2, and H3K4me3 protein, we performed ChIP analysis using anti-Ago2, Oct4, MBD6, AcetylH3, AcetylH4, H3K4me2, and H3K4me3 antibodies. For this study, anti-Ago2, Oct4, and MBD6 monoclonal antibodies were obtained from Santa Cruz Biotechnology, and anti-AcetylH3, AcetylH4, H3K4me2, H3K4me3, and a rabbit immunoglobulin G (IgG; PP64B) antibody were obtained from Millipore. Cells were harvested and chemically cross-linked with 1 % formaldehyde (Sigma) for 20 h at 4 °C. Fixation was quenched by incubation in 2.5 M glycine for 5 min at room temperature. Cells were pelleted at 4 °C (500 *g*), washed with ice-cold phosphate buffered saline (PBS) and lysis buffer (10 mM Tris–HCl, 10 mM NaCl, 3 mM MgCl2, 0.5 % GEPAL, 1 mM fresh PMSF), pelleted, and flash-frozen in liquid nitrogen. The cell pellets were resuspended in pre-IP dilution buffer containing 4 % GEPAL and 1 mM PMSF. The cells were then sonicated using a Branson Sonifier 450D (Branson Ultrasonics, Danbury, CT) at 50 % amplitude with 1-min rests in ice water. The sonicated fragments ranged in size from 200 to 1,000 bp. Post-sonication, the samples were centrifuged at 14,000 rpm for 10 min at 4 °C and flash-frozen in liquid nitrogen.

Sonicated cell extracts equivalent to 2×10^6 cells were used for the immunoprecipitations. Samples were precleared with protein G Dynabeads (Dynalabs, St. Louis, MO) in 1,000 ml dilution buffer (0.01 % SDS, 1.1 % Triton X-100, 1.2 mM EDTA, 16.7 mM Tris–HCl, pH 8.1,, 167 mM NaCl, Upstate protease inhibitor cocktail II). To induce chromatin and specific antibody binding against Ago2, Oct4, and MBD6 protein, cell extracts were incubated with 1 mg antibody overnight at 4 °C. The chromatin–antibody complexes were isolated with protein G Dynabeads and washed one time with low salt buffer (0.1 % SDS, 1 % Triton X-100, 2 mM EDTA, 20 mM Tris–HCl, 150 mM NaCl), one time with high salt buffer (same as low salt but with 500 mM NaCl) and twice with TE. Protein/DNA complexes were eluted from the beads in 10 ml 20 % SDS, 20 ml 1 M $NaHCO_3$ and 170 ml H_2O at 65 °C with occasional vortexing. The cross-linking was reversed by the addition of 8 ml 5 M NaCl and incubation overnight at 65 °C. The extracts were then treated with RNase A and proteinase K, and the DNA was purified using an Upstate EZ ChIP kit. For DNA amplification, a total of 5 mg of purified DNA (Ago2-chip, Oct4-chip, MBD6-chip, and Input) was amplified using a GenomePlexH Whole Genome Amplification (WGA) kit (Sigma). Amplified DNA was used for the ChIP–PCR analysis.

Whole mount in situ analysis

In situ hybridization was performed on cultured hATSCs. Several different microRNA oligonucleotide probes were synthesized (Dharmacon RNA Technologies). Tissue slides were air dried and prepared for 15 min in a saline citrate solution (pH 7.0) containing 0.1 mg/ml proteinase K (Sigma–Aldrich, St. Louis, MO) at room temperature. Sections were washed two times in 1× SSC for 5 min. Labeled oligonucleotides were diluted (30 pM) in a hybridization buffer containing 50 % de-ionized formamide, 4× SSC, and 1 mM sodium pyrophosphate, covered with parafilm, and incubated in a humid chamber overnight at 42 °C. Following the incubation, the sections were rinsed for 10 min in 1× SSC at RT, for 20 min in 1× SSC at 60 °C, and for 5 min in distilled water at room temperature (RT), then dehydrated through a graded series of 70, 95, and 100 % isopropanol, and finally air-dried. The controls in which specific probes were omitted resulted in no detectable staining. The specimens were evaluated using a Leica fluorescence microscope (Leica Microsystems, Exon, PA). These studies were repeated at least three times.

Differentiation potencies of hATSCs

In order to compare the multipotential differentiation abilities of hATSCs, the cells were subjected to differentiation under known conditions to induce adipogenic, osteogenic, and chondrogenic lineages in human cells. Prior to culturing in the induction media, the cultures were grown to confluence. For adipogenic differentiation, the hATSCs were induced by passage at a dilution of 1:10 in control media supplemented with 10 ng/ml of insulin and 10^{-9} M dexamethasone (Sigma). Adipogenic differentiation was visualized by the presence of highly refractory intracellular lipid droplets via phase-contrast microscopy. In order to induce osteogenic differentiation, the cultures were fed daily for 3 weeks with control medium to which 10 mM β-glycerophosphate, 50 ng/ml ascorbic acid, and 10^9 M dexamethasone had been added. The mineralization of the extracellular matrix was visualized by the staining of the cultures with von Kossa and Alizarin Red. Von Kossa staining was conducted using an aqueous 5 % $AgNO_3$ solution, followed by 2 min of fixation in 5 % $Na_2S_2O_3$ solution. For chondrocyte differentiation, a pellet culture system was utilized. Approximately 3×10^6 de-ATSC and ATSC controls were placed in the wells of a 96-well plate. The pellet was cultured at 37 °C with 5 % CO_2 in 500 ul of chondrogenic media containing 6.25 g/ml insulin, 10 ng/ml of transforming growth factor 1, and 50 ng of ascorbate-2-phosphate in control media for 2–3 weeks. The medium was replaced every 2 days for 15 days.

Senescence associated beta-gal staining

We use a manual protocol when staining for senescence associated beta-gal (SA-β-gal). The staining solution was composed of 100 mM $K_3Fe(CN)_6$, 1 M $MgCl_2$, 5 M NaCl, 0.1 M citric acid containing 0.2 M sodium phosphate dibasic (Na_2HPO_4) at pH 6.0, 100 mM $K_4Fe(CN)$, 20 mg/ml of X-gal solution dissolved in DMF (dimethylformamide) in PBS. The fixative solution consisted of 2 % formaldehyde with 0.2 % glutaraldehyde in PBS, pH 7.2. After a brief wash with PBS, cells were fixed with 1× fixative solution for 10 min, then washed twice with PBS, and stained with staining solution in 37 °C overnight. Cells were visualized with a microscope for development of blue color.

Luciferase assay

To measure the promoter activity, we purchased the Bright-Glo™ Luciferase Assay System and pGL3 Enhancer vector (Promega) and designed primers containing the restriction enzyme sites as follows: 5′-overhang of forward primer has the *Nhe*I site, and the 3′-overhang of the reverse primer has the *Hin*dIII sites for Oct4 and MBD6. For the Ago2 promoter construction, we designed primers containing the restriction enzyme sites as follows: the

5′-overhang of the forward primer has the *Nhe*I site, and the 3′-overhang of the reverse primer has the *Xho*I sites. The primers so constructed were: Pro-Oct4-F1 (CTAGCTAGC GCTCAGCCAATAACTCA), Pro-Oct4-R1 (AAGCTT GGGCAAGTATAGGGCTTGT), Pro-Ago2-F1 (NCTTAG CACCCACGGAGAGCAGGATGGAG), Pro-Ago2-R1 (CCGCTCGAGCAACACAGCGCTCAAAGGAGCTGA AG), Pro-MBD6-F1 (CTAGCTAGCGGACCCCAAAA CCTACCAAT), and Pro-MBD6-R1 (AAGCTTGGG GGGCCAAGAAATATGGGAGT).

PCR was performed to amplify the promoter region of Ago2, MBD6, and Oct4 genes. Insert and vector were double digested by *Nhe*I and *Hin*dIII (Promega) and the fragments extracted from the gel by HiYield Gel/PCR DNA Fragments Extraction kit (RBC Bioscience, Taipei, Taiwan). Ligation was mediated by T4 ligase (Promega) at 23°, 20°, 17°, and 4° C, respectively, for 1 h, and the ligation products were transformed to HIT^{TM}-DH5α, competent cell (RBC Bioscience). For the luciferase promoter assay, cells were seeded in 6-well plates until 70 % confluence and transfected with Ago2, MBD6, or Oct4 using Lipofectamine^{TM}. Cells were transfected with a pair of reporter gene plasmids using Lipofectamine^{TM} LTX and Plus^{TM} Reagent, referring to the manufacturer's protocol (Invitrogen). After transfection of each plasmid, cells were incubated with DMEM containing 10 % FBS. At 24–48 h post-transfection, the medium was replaced with fresh phenol red-free RPMI plus 0.1 % bovine serum albumin (BSA) with 10 nM DHT. Cells were harvested 24–48 h later for dual luciferase assays (Bright Glo; Promega) to determine the promoter activity of the test plasmid. Firefly luciferase expression from the test plasmid and Renilla luciferase expression from phRL-SV40 in a single sample were measured sequentially in a luminometer according to the Dual-Luciferase Reporter System protocol (Bright Glo; Promega).

Statistical analysis

Significance was tested by the *t* test or ANOVA using InStat ver. 3.0 software (GraphPad Software, San Diego, CA). For repeated measures, ANOVA with appropriate post hoc tests. For in vitro studies where Kaplan–Meier curves and log-rank analyses were performed, MedCalc software (MedCalc Software, Mariakerke, Belgium) was used.

Results

Ago2 enhanced the stemness gene expression and cell proliferation

We assessed the effect of Ago2 on the behavior of human adipose tissue-derived stem cells. Ago2-transfected cells were harvested after 48 h according to our previously published conditions (Fig. 1). The introduction of exogenic Ago2 increased cell number and compaction. In contrast, knockdown of Ago2 expression induced cell growth attenuation and finally resulted in massive cell death (Fig. 1a). We also measured cell proliferation using a nuclear bromodeoxyuridine (BrdU) incorporation assay (Fig. 1a). As predicted, the cellular level of BrdU coincided with the morphological differences induced by Ago2. To further study the effect of Ago2 on the expression of various functional genes, we performed reverse transcriptase (RT)-PCR. Oct4, Sox2, Nanog, and Klf4 mediate cellular reprogramming into a more primitive state. Expression levels of these mRNA transcripts and of growth-associated genes were increased by Ago2 overexpression and significantly reduced by the interference of Ago2 expression (Fig. 1c–e). Ago2 promoted its own expression and positively regulated Oct4 expression, leading us to conclude that Ago2 has regulatory roles in stemness activation directly for Oct4 and indirectly for Sox2, Nanog, Klf4, and Rex1 (Fig. 1d). Expression of cell cycle regulators, such as CDK2, CDK4, and RUNX3 also correlated with Ago2 expression levels (Fig. 1e). These results demonstrate that Ago2 activates stemness and proliferation at both morphological and transcriptional levels. We next identified Ago2 nuclear localization by immunocytochemistry and analyzed Ago2-binding target genes via ChIP-PCR analysis (Fig. 2a, b). Ago2 and Oct4 were detected as target genes of nuclear Ago2 (Fig. 2c). These results indicate that Ago2 regulates self-renewal by positively controlling gene expression of Oct4 and Ago2 through binding to the promoter region of both Oct4 and Ago2 (Fig. 2d). To further study the related gene regulation network, we constructed a luciferase vector system to establish whether Ago2 directly controls Oct4. Following the luciferase assay result, we confirmed direct regulation of Ago2 for Oct4 (Fig. 2d) [2, 8, 29].

Oct4 directly controls MBD6 expression and MBD6-mediated cell proliferation

Our previous study demonstrated that Oct4 functions in the self-renewal, proliferation, and survival of hATSCs [10]. Oct4 expression stimulated cell proliferation in hATSCs (Fig. 3a) and regulated the expression of stemness genes, REST, and cell cycle-related genes. Overexpression of Oct4 significantly increased the expression of Ago2 and MBD6, while Oct4 depletion effectively downregulated Ago2 and MBD6 expression (Fig. 3b–e). ChIP-PCR sequencing revealed that MBD6 was also bound to the regulatory region of the MBD6 gene and directly controlled MBD6 expression (Fig. 3f, g). We also detected Oct4 bound to specific sequences in the regulatory regions

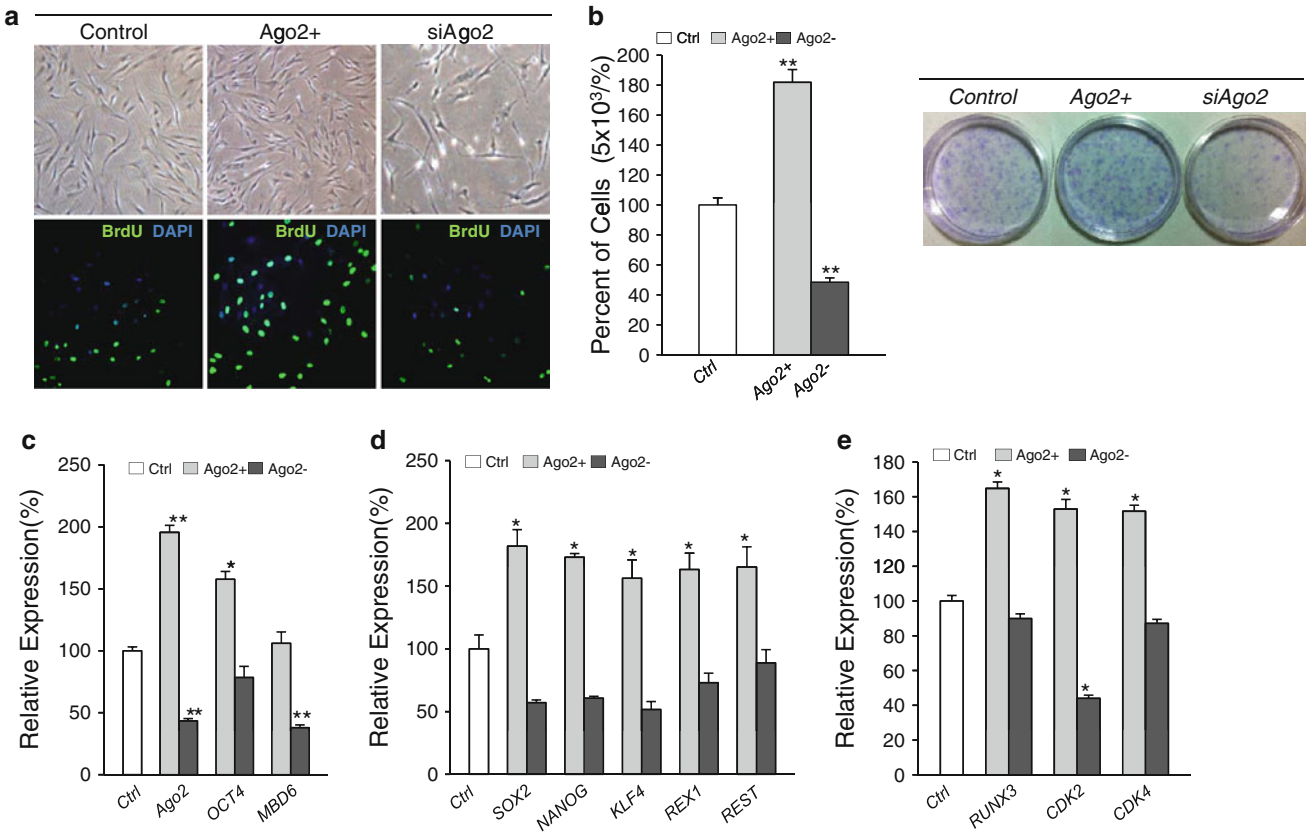

Fig. 1 Nuclear Argonaute 2 (*Ago2*) regulation of stemness and cell cycle-regulating gene expression during the self-renewal of human adipose tissue-derived stem cells (hATSCs). **a**, **b** Proliferation activity of Ago2-overexpressing (*Ago2*+) or Ago2-depleted (*Ago2*− or siAgo2) cells. For the evaluation of cell proliferation, bromodeoxyuridine (*BrdU*) staining (**a**) and trypan blue exclusion assays (**b**) were performed. For detecting self-renewal activity in hATSCs, a single cell-derived colony forming unit (CFU) was evaluated. **c** Expression of Ago2 and putative Ago2-regulating genes [Ago2, octamer-binding transcription factor 4 (Oct4), and methyl-CpG-binding domain 6 (MBD6)] were controlled by Ago2. **d** Overexpression or interference of Ago2 expression significantly affected stemness gene and REST expression in hATSCs. **e** Overexpression or interference of Ago2 expression altered CDK2, CDK4, and RUNX3 expression in cultured hATSCs. $*P < 0.05$, $**P < 0.01$ vs. the naïve control group. *Ctrl* Control

of Oct4 and MBD6 (Fig. 3g), leading us to investigate the expression of Oct4 and MBD6 using a luciferase assay. Oct4 overexpression enhanced luciferase activity driven by the Oct4 and MBD6 promoters in hATSCs (Fig. 3h). Due to differential expression levels of Oct4 and MBD6 in various passages of hATSCs, we used late passage cells (p15) for MBD6 overexpression and early passage cells (p8) to study MBD6 regulation of proliferation and functional gene expression of hATSCs (Fig. 4a). We found that Ago2, Oct4, and MBD6 expression gradually increased until P12, but that MBD6 expression gradually decreased after P13 (Fig. 4b). Compared to control cells, cells overexpressing MBD6 showed a significantly increased growth activity. In contrast, knockdown of MBD6 resulted in decreased growth activity (Fig. 4c, d). To confirm that MBD6 functions in cell proliferation, we performed a FACS (fluorescence-activated cell sorting) analysis of the S phase cell population. When MBD6 was overexpressed, cells showed an extensible high S phase compared to normal cells (Fig. 4d). Moreover, the results of the FACS analysis showed that overexpression of MBD6 gene expression was significantly increased in the S phase of the cell population (Fig. 4d). To evaluate the effect of MBD6 knockdown on cell self-renewal and senescence, we performed BrdU and SA-β-gal staining. Reducing MBD6 expression resulted in a considerable decrease in proliferating BrdU-positive cells, whereas SA-β-Gal-positive senescent cells significantly increased (Fig. 4e). Additionally, RT-PCR and immunochemical analysis showed significantly reduced expression levels of stemness and cell cycle regulators, as previously mentioned. After MBD6 knockdown, cells were markedly reduced in size and eventually died. In contrast, there was a high-density population of MBD6-overexpressing cells that were spindle-shaped and had traditional mitotic cell morphology (Fig. 4e). To observe the effect of MBD6 on cell senescence, proliferation, and stemness gene expression, we performed RT-PCR analysis, immunocytochemistry, and

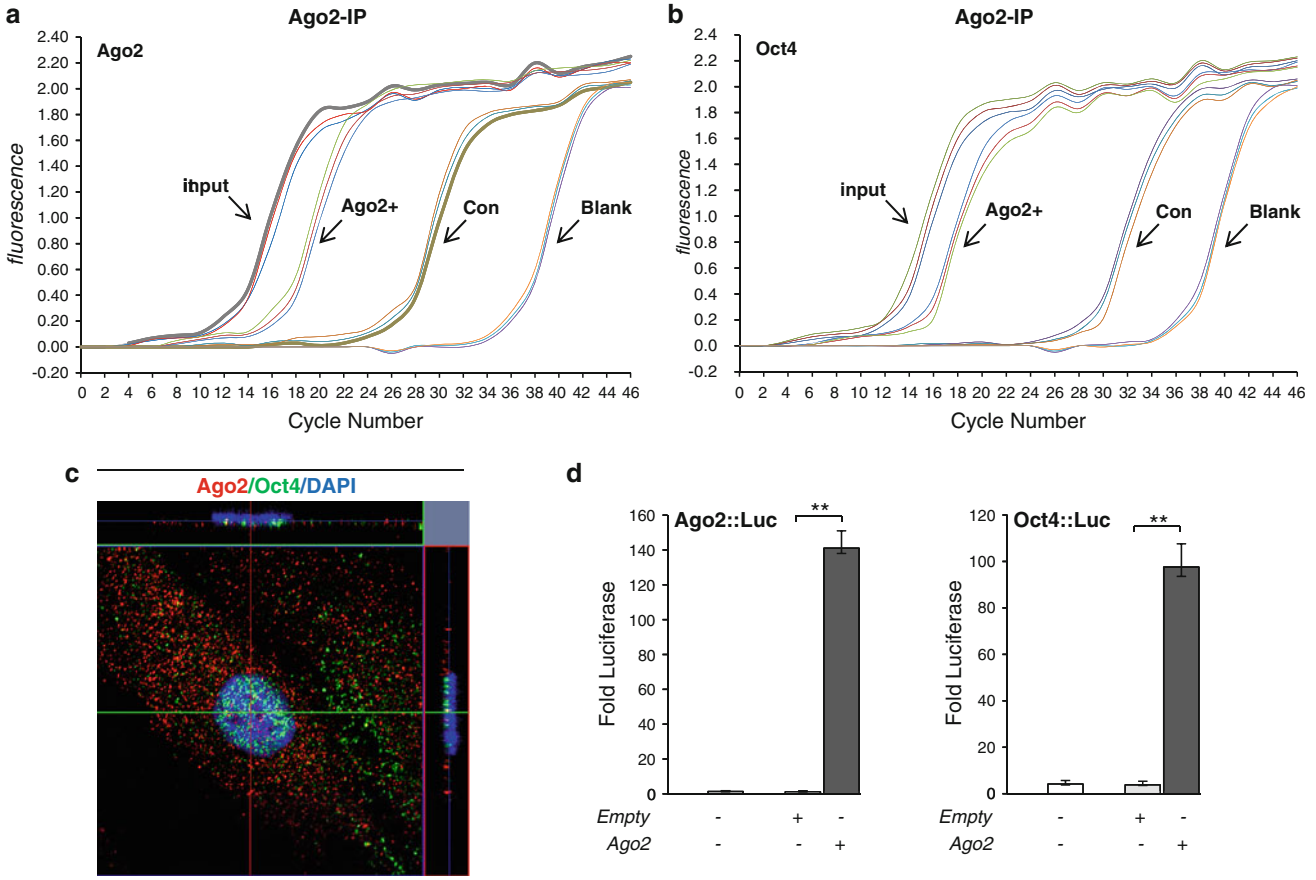

Fig. 2 Binding of Ago2 on the regulatory regions of Ago2 and Oct4 directed gene expression in hATSCs and cell proliferation. **a**, **b** Confirmation of nuclear localized Ago2 and analysis of Ago2 binding and relative enrichment of Ago2 and Oct4 promoter regions by Ago2 ChIP/PCR expressed as log2 enrichment over the input and fold change of Ago2 binding frequency on the promoter region of the Ago2 and Oct4 genes before and after Ago2 overexpression in hATSCs. **c** Immunocytochemical analysis revealed nuclear colocalization of Ago2 and Oct4. **d** Luciferase activity of Ago2 and Oct4 is promoted by Ago2 overexpression in hATSCs. Ago2 and Oct4 are promoted by Ago2 overexpression in hATSCs. Ago2 and Oct4 promoter luciferase activity significantly increased by Ago2. $^{**}P < 0.01$ vs. the naïve control group. *IP* Immunoprecipitation

SA-β-Gal staining (Fig. 4e–h). The RT-PCR results demonstrated that reprogramming factors, such as Oct4, Sox2, Nanog, Klf4, and other cell cycle regulators (i.e., Rex1, Rest, Runx3, CDK2, and CDK4), were upregulated after MBD6 overexpression in hATSCs. We confirmed this result using immunocytochemical staining for Oct4, Sox2, and Nanog in hATSCs with increased expression of MBD6 (Fig. 4f, h). Moreover, MBD6 overexpression enhanced luciferase activity driven by the Oct4 or MBD6 promoters in hATSCs (Fig. 4i). MBD6 was bound to specific sequences in the regulatory regions of Oct4 and MBD6 genes. Additionally, we investigated the mRNA expression levels of Ago2, MBD2, MBD3, MBD4, BRCA2, and USP44 before and after overexpression or interference of MBD6 (Fig. 4j, k). We also found that MBD6 directly regulated MBD2, MBD3, MBD4, STAT3, USP44, BRCA2, REST, and β-catenin by direct binding on regulatory regions of these genes in hATSCs (Fig. 4l). The binding frequency of β-catenin, REST, MBD3, USP44, and BRCA2 was more or less higher than that of other functional genes (Fig. 4l).

MBD6 controls functional gene clusters at the protein level

To elucidate how MBD6 regulates several clusters of functional genes, we performed western blot analysis before and after MBD6 overexpression or knockdown and quantified the expression of these functional genes at the protein level (Fig. 5a–d). MBD6 overexpression in late passage hATSCs induced upregulated expression of stemness genes and c-Myc, whereas interference of MBD6 expression in early passage hATSCs significantly downregulated the expression of stemness genes, Oct4, Sox2, Nanog, and Rex1 (Fig. 5a). In contrast, the expression of the cell death signal involving the mediators p53, p21, and

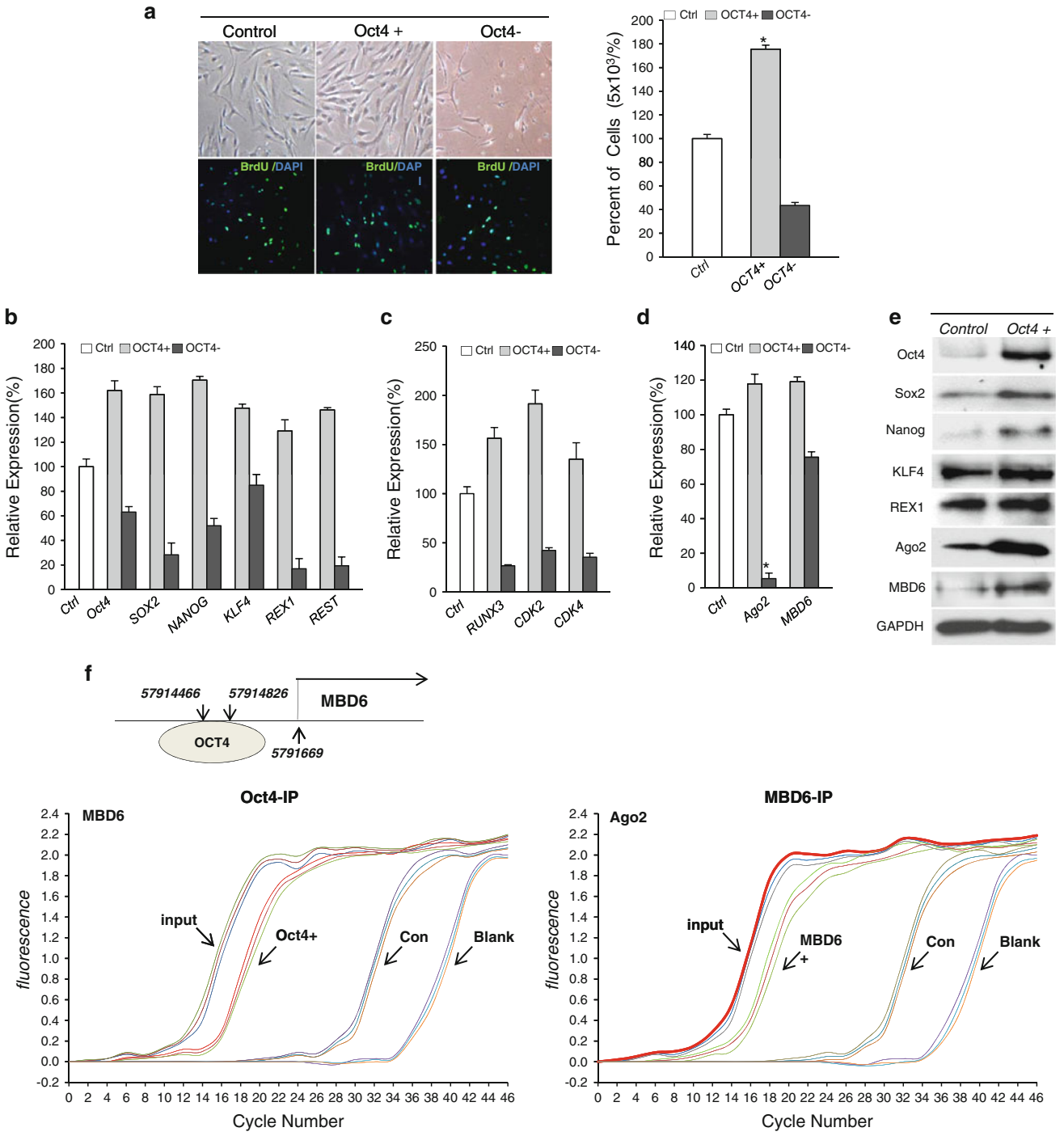

Fig. 3 Oct4-mediated hATSC proliferation and functional gene expression. **a** The effect of Oct4 expression on hATSC proliferation. Phase contrast image analysis and BrdU staining demonstrated that Oct4 overexpression effectively increases cell proliferation. **b**, **c** Overexpression or interference of Oct4 expression significantly upregulated or downregulated stemness gene, REST, and cell cycle-related gene expression, in the transcriptional level respectively. **d** Overexpression of Oct4 effectively induces increased expression of Ago2 and MBD6 in hATSCs. **e** Western blot analysis result revealed that overexpression of Oct4 expression significantly upregulated in the protein level of stemness genes, MBD6, and Ago2 expression. **f** MBD6 directly binds the promoter regions of MBD6, as shown by ChIP-PCR expressed as log2 enrichment over the input. Additionally, Ago2 ChIP analysis revealed that Ago2 also directly bound to the promoter region of MBD6 gene. **g** Putative Oct4 binding sites on MBD6 genome. **h** Luciferase activity was significantly increased in pmirGlo-MBD6-wt/pcDNA-Oct4 gene-transduced group compared to pmirGlo-MBD6-wt control groups. Luciferase assay of Oct4 or MBD6 promotor construct revealed that Oct4 directly controls Oct4 and MBD6 gene expression after binding to regulatory region of Oct4 and MBD6 gene in hATSC. $*P < 0.05$, $**P < 0.01$ vs. the naïve control group

Fig. 3 continued

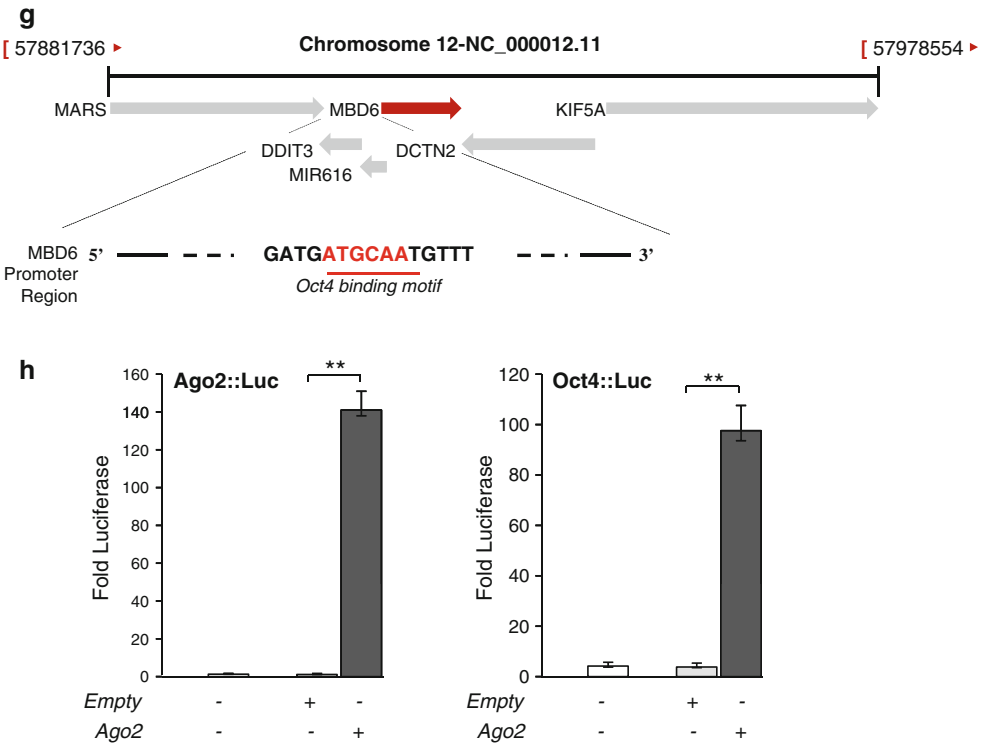

c-Myc was significantly decreased and increased at each passage (Fig. 5b). In addition, phosphorylation of JNK/p38, JAK/STAT3, PI3K/AKT, ERK1/2, and Wnt 5A/β-catenin signaling proteins was significantly increased (Fig. 5c). Although previous studies reported that MBD6 does not directly interact with methylated CpG DNA, we expected that it may influence the methylation state indirectly via acetylation- and methylation-mediating gene expression. Acetylation is generally an epigenetic marker of active chromatin (euchromatin), suggesting an active transcriptional state. In contrast, DNA methylation represses transcription. Indeed, we found that acetyl H3, H4, and H3K4me3 increased after MBD6 overexpression (Fig. 5d). On the other hand, via the ChIP analysis using anti-acetyl H3, acetyl H4, H3K4me2, and H3K4me3 antibodies, we also detected that epigenetic machinery directly controlled Oct4 and MBD6 expression. As shown in Fig. 5d, Oct4 expression was directly regulated by acetyl H3, acetyl H4, H3K4me2, and H3K4me3, or indirectly, and MBD6 expression also indirectly affected Oct4 expression. Moreover, the significantly increased binding affinity of acetyl H3 and acetyl H4 to the regulatory region of Oct4 was detected in cultured hATSCs. In contrast, the binding affinities of H3K4me2 and H3K4me2 to the promoter region of the Oct4 gene was not affected by MBD6 expression (Fig. 5d). We are also analyzed methylation

Fig. 4 Involvement of MBD6 in deaging and cell proliferation of hATSCs via direct Oct4 regulation. **a**, **b** MBD6, Oct4, and Ago2 differential expression at various passages (*p15*, *p8*) in cultured hATSCs. At early passages, MBD6, Oct4, and Ago2 expression gradually increased, but after passage 12 (late passage), gene expression significantly decreased. **c–e** MBD expression effectively enhanced cell proliferation. Cell proliferation activity [BrdU+ and fluorescence-activated cell sorting (FACS) analysis results] significantly increased after MBD6 overexpression in hATSCs. Cell aging factor β-galactosidase (β-*gal*) expression was significantly decreased in MBD6-overexpressing cells. **f**, **g** Overexpression of MBD6 significantly enhanced expression of cell cycle-related and stemness genes in hATSCs at the transcriptional level. **h** Immunocytochemical analysis in hATSCs following MBD6 overexpression or interference revealed that the expression of Oct4, Sox2, and Nanog significantly increased after MBD6 overexpression. **I** Luciferase activity of MBD6 or the Oct4 promoter before and after MBD6 overexpression in hATSCs. Ago2 was also directly bound to MBD6 promoter for increased MBD6 expression in hATSCs. For MBD6 and Oct4 luciferase assay, cells were transfected with pGL3-PSA, a phRL-SV40 plasmid. The results show that MBD6 and Oct4 promoter binding activity was significantly increased by MBD6. **j**, **k** The effect of Ago2, MBD2, MBD3, MBD4, BRCA2, and USP44 expression before and after MBD6 overexpression or interference in hATSCs. **l** Direct control of MBD6 on regulatory regions of MBD6, MBD2, MBD3, MBD4, STAT3, USP44, BRCA2, REST, and β-catenine for the regulation of their gene expression in MBD6-overexpressed hATSCs culture and fold change of MBD6 binding frequency on the promotor region of MBD6, MBD2, MBD3, MBD4, STAT3, USP44, BRCA2, REST, and β-catenine genes before and after MBD6 overexpression in hATSCs. $^{*}P < 0.05$, $^{**}P < 0.01$ vs. the naïve control group

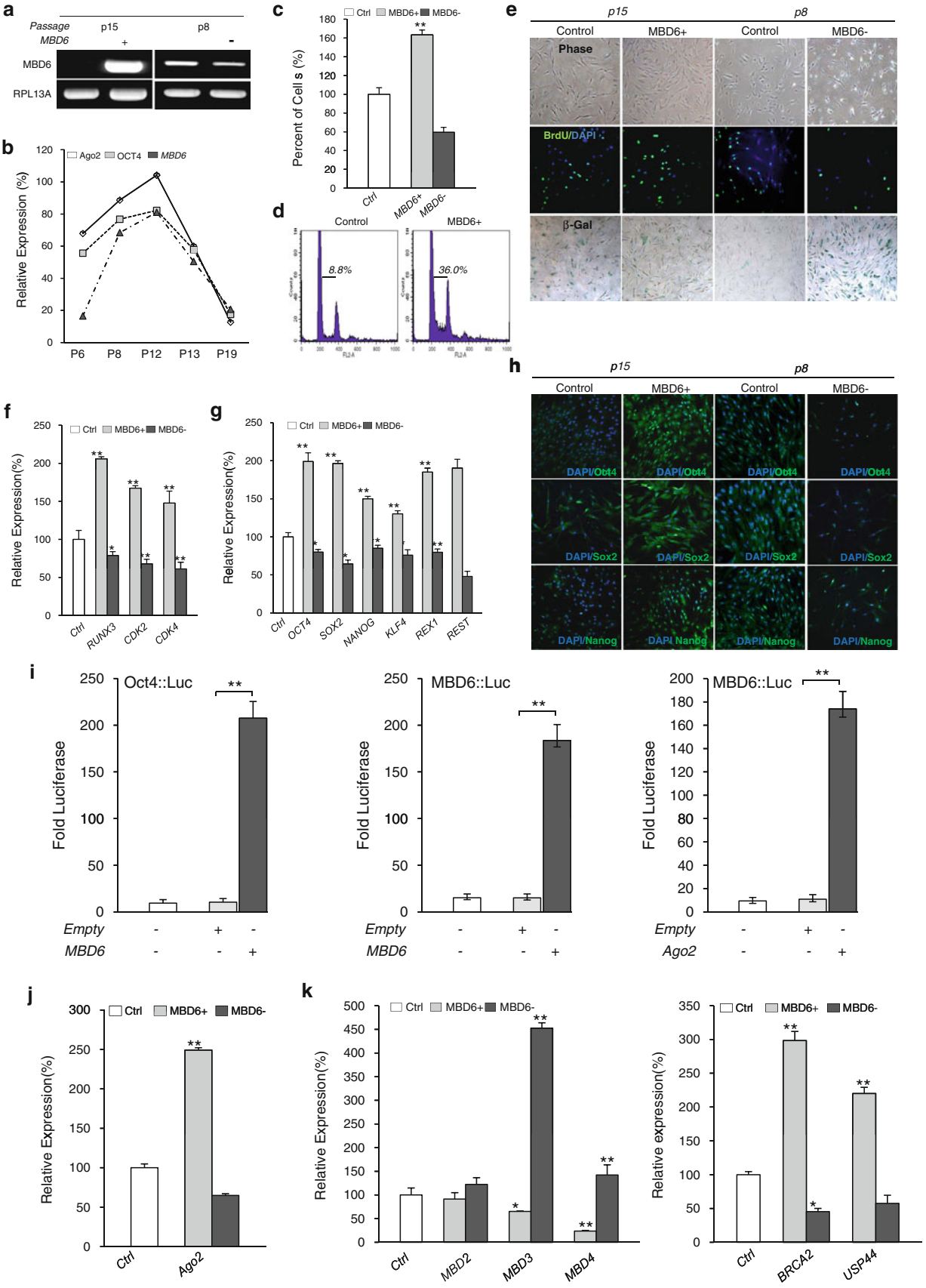
a
Passage
MBD6
p15
p8
+
-
MBD6
RPL13A
b
Ago2
OCT4
MBD6
Relative Expression (%)
P6
P8
P12
P13
P19
c
Ctrl
MBD6+
MBD6-
Percent of Cell s (%)
d
Control
MBD6+
8.8%
36.0%
e
p15
p8
Control
MBD6+
Control
MBD6-
Phase
BrdU/DAPI
β-Gal
f
Relative Expression(%)
RUNX3
CDK2
CDK4
g
OCT4
SOX2
NANOG
KLF4
REX1
REST
h
DAPI/Oct4
DAPI/Sox2
DAPI/Nanog
i
Oct4::Luc
MBD6::Luc
Fold Luciferase
Empty
MBD6
Ago2
j
Relative Expression(%)
Ago2
k
MBD2
MBD3
MBD4
BRCA2
USP44
Relative expression(%)

Fig. 4 continued

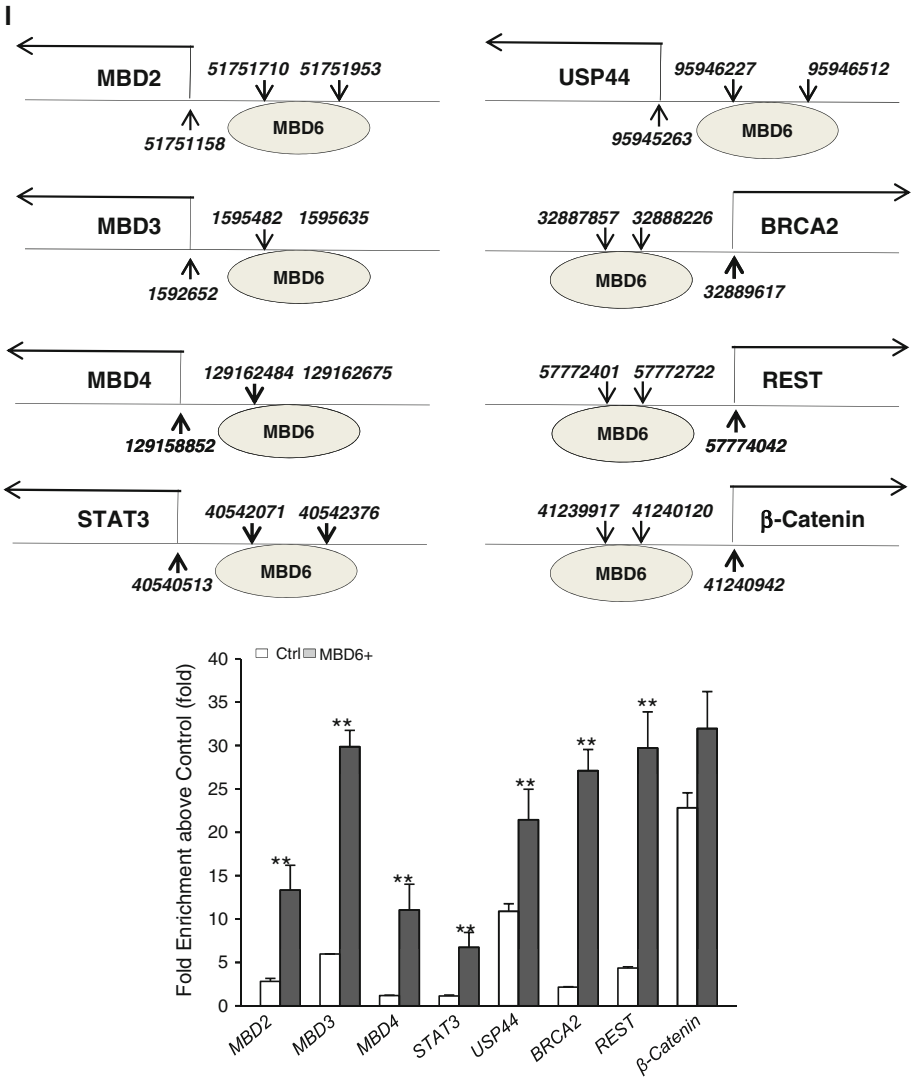

with bisulfite sequencing and observed a reduction (approx. 20 %) of methylation following MBD6 overexpression (Fig. 5e).

MBD6 overexpression significantly enhances the differentiation potency of hATSCs

Pluripotency is a representative ability of embryonic stem cells that allows them to differentiate into the three germ layers (endoderm, mesoderm, and ectoderm). To study the effect of MBD6 on pluripotency, we evaluated the differentiation potency of control and MBD6-overexpressed hATSCs (Fig. 6). Due to the differential expression level of MBD6 in hATSC cells at various passages, we used late passage cells (p15) to study MBD6 overexpression and early passage cells (p8) to study MBD6 regulation of hATSC differentiation into mesodermal lineage and related gene expression. To induce differentiation into fat, chondrocytes, or bone, we incubated hATSCs in the lineage-specific differentiation induction medium. We assessed differentiation potency by comparing phenotypic characteristics and the expression of bone, fat, and cartilage-specific genes at the transcriptional level. After the cells had been induced to differentiate into the three germ layers of tissue (bone, fat, and cartilage, respectively) for at least 2 weeks, the cells were stained with a dye appropriate for each tissue type. We subsequently observed differences in staining intensity after MBD6 overexpression or knockdown of MBD6 in hATSCs compared to the control group. Differentiated MBD6 overexpressing cells showed fainter Oil Red O staining than control cells, suggesting that MBD6 expression attenuated fat differentiation in hATSCs. Consistent with these results, knockdown of MBD6 expression resulted in more intense Oil Red O staining compared to control cells (Fig. 6a). Similar results were observed with toluidine blue O and silver nitrate staining, which are dyes for chondrocytes and bone, respectively. Therefore, we concluded that MBD6 inhibits mesodermal

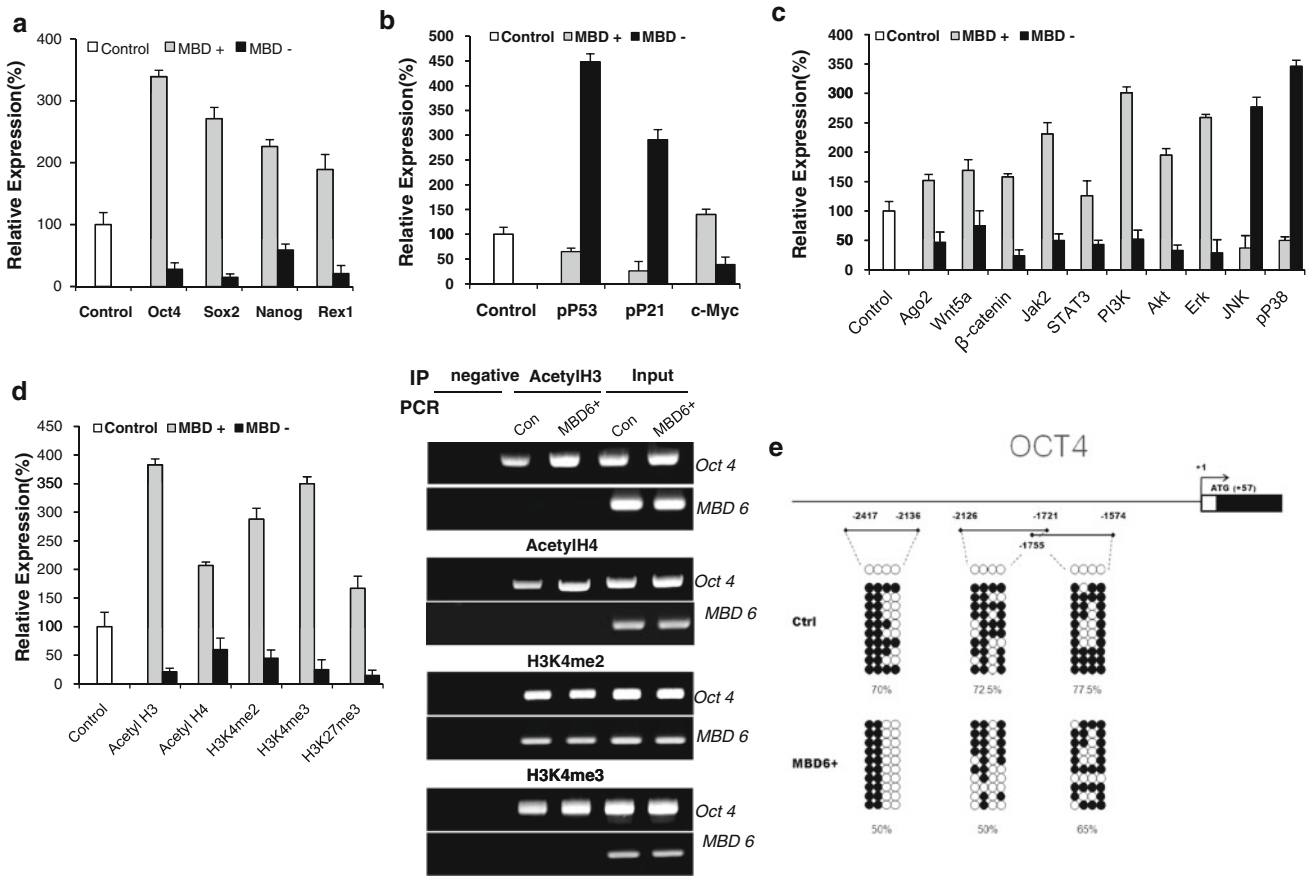

Fig. 5 The effect of MBD6 overexpression on the phosphorylation of P38/JUNK, JAK/STAT3, and Wnt5a/β-catenin as well as the methylation or acetylation status involving functional gene expression in hATSCs. **a** MBD6 overexpression in late passage of hATSCs, **b** increased stemness gene expression, while MBD6 depletion (passage 15) significantly decreased stemness gene expression at passage 8 along with c-Myc upregulation and p53 downregulation. **c** MBD6 overexpression at passage 15 of hATSCs resulted in significantly decreased JUNK/P38 phosphorylation and p21 downregulation. Moreover, JAK/STAT3 and PI3 K/AKT phosphorylation significantly increased after MBD6 overexpression, resulting in prominently decreased phosphorylation of JAK/STAT3 and PI3 K/AKT phosphorylation along with reduced Wnt5a and β-catenin activation. **d** Methylation or acetylation of histones 3 and 4 was altered by the MBD6 expression level. Interference expression of MBD6 (at passage 8) or overexpression of MBD6 (at passage 15) effectively induces acetylated H3 and H4 reduction and elevation, respectively. H3Kme, H3Kme3, and H3K27me3 expression also significantly increased following MBD6 overexpression in hATSCs at passage 15. ChIP/PCR analysis of Oct4 and MBD6 against anti-acetylH3, acetylH4, H3K4me2, and H3K4me3 antibodies before and after MBD6 overexpression in cultured hATSCs. **e** Differential methylation pattern of Oct4 before or after MBD6 overexpression in hATSCs

differentiation (Fig. 6a, b). To validate these phenotypic results, we analyzed lineage-specific gene expression. Peroxisome proliferator-activated receptor gamma (PPARγ), a genetic marker of adipose tissues, was downregulated after MBD6 overexpression and significantly increased after inhibition of MBD6 expression (Fig. 6b). Osteonectin (bone marker) and collagen type IV (differentiated chondrocyte marker) showed similar patterns of gene expression as PPARγ before and after MBD6 differential expression (Fig. 6b, c). Thus, the gene expression patterns and phenotypic analyses both indicated that MBD6 significantly attenuates the ability of hATSCs to differentiate into the mesodermal lineage. We are also detected an effect of the MBD6 gene on Sca1 and CD31 expression. As shown in Fig. 6d, MBD6 expression did not affect Sca1+ and CD31+ population density (Fig. 6d). On the other hand, the expression of the neural development-related genes PAX6 (paired box gene 6) and homeobox protein HOXB4 was significantly increased after MBD6 overexpression (Fig. 6e). We also examined the effect of MBD6 expression on neural differentiation by evaluating sphere formation efficiency and, neural lineage-related gene expression by RT-PCR and immunocytochemical analysis of differentiated cells (Fig. 6f, g). Sphere size was larger in cells that overexpressed MBD6 compared with control cells. In contrast, MBD6 knockdown cells did not form sphere-like neural precursors (Fig. 6f). Early neuronal marker beta III tubulin (TUJ) and the astrocyte marker glial fibrillary acidic protein (GFAP) were also elevated after MBD6 overexpression (Fig. 6g, h). Microtubule-associated

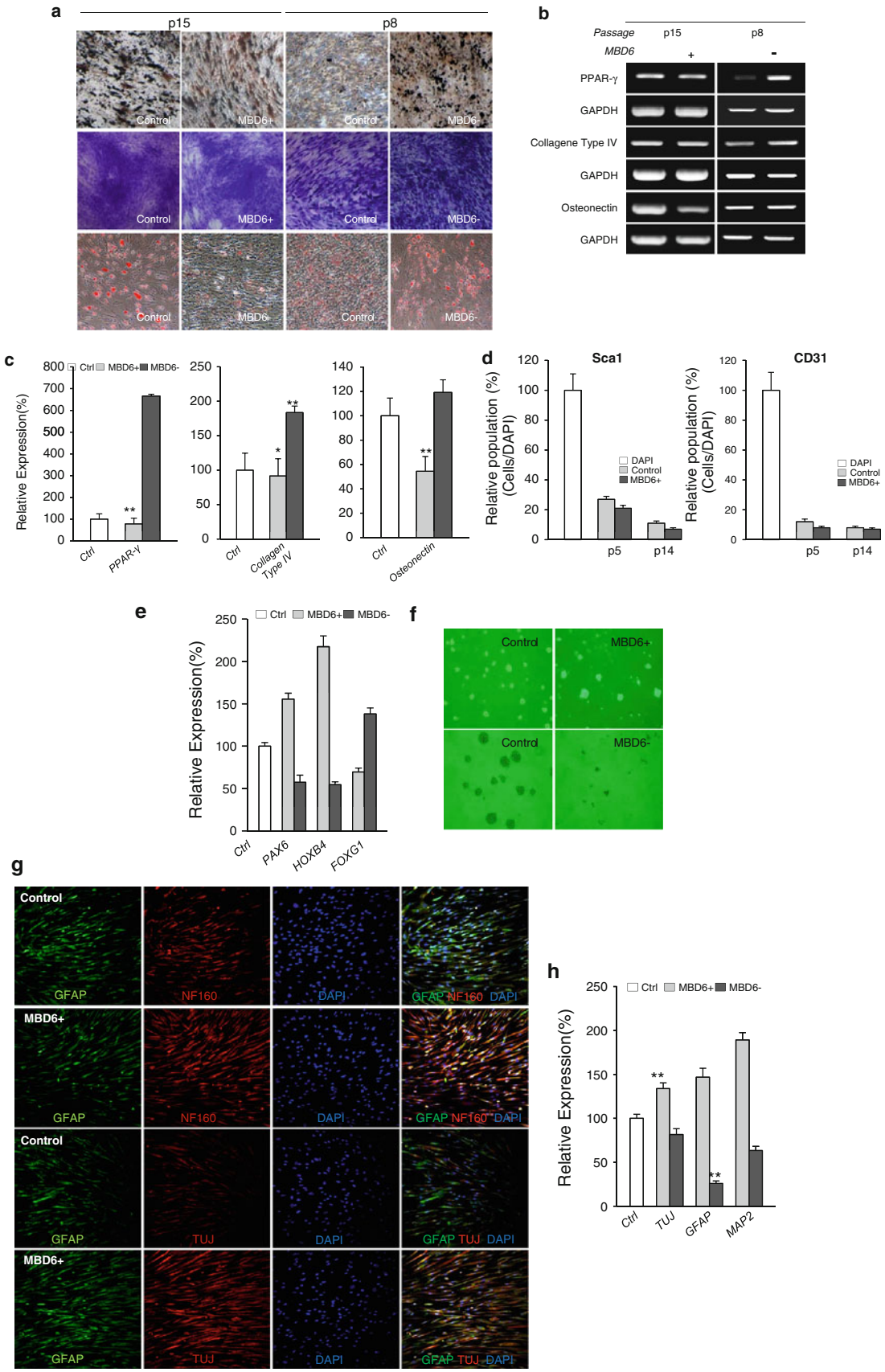
a
p15
p8
Control
MBD6+
MBD6-
b
Passage
MBD6
PPAR-γ
GAPDH
Collagene Type IV
Osteonectin
c
Relative Expression(%)
Ctrl
MBD6+
MBD6-
PPAR-γ
Collagen Type IV
Osteonectin
d
Sca1
CD31
Relative population (%) (Cells/DAPI)
DAPI
Control
MBD6+
p5
p14
e
Relative Expression(%)
PAX6
HOXB4
FOXG1
f
g
GFAP
NF160
TUJ
DAPI
h
TUJ
GFAP
MAP2

◀ **Fig. 6** Exogenic expression of MBD6 effectively attenuated differentiation in the mesodermal linage, while the ability for neural differentiation significantly increased in vitro. **a** Mesodermal differentiation potential of MBD6+ hATSCs (p15) and siMBD6-treated hATSCs (p8) compared with control hATSCs. Ectopic HSP60-treated hATSCs were stained for differentiated cartilage, fat, and bone. **b**, **c** RT-PCR analysis of lineage-specific gene expression after bone, fat, and cartilage differentiation of MBD6+ hATSCs and siMBD6-treated hATSCs compared with control hATSCs. $^{**}p < 0.01$, $^{*}p < 0.05$ ($n = 5$). ANOVA was used for comparisons with control cells. **d** The effect of MBD6 expression on hematopoietic lineage of cells expressing Sca1 and CD31 in hATSCs. **e**, **f** The effect of MBD6 expression on neural development-related gene expression (**e**) and neurosphere formation efficiency (**f**). MBD6 effectively enhances neurosphere formation after neural induction in hATSCs culture. **g**, **h** After induction neural differentiation in MBD6+ hATSCs, neurospheres effectively differentiated into neuronal cells and astrocytes that expressed TuJ, NF160, and GFAP. These data were confirmed by immunocytochemical analysis. $^{*}P < 0.05$, $^{**}P < 0.01$ vs. the naïve control group

protein 2 (MAP2), a mature neuronal marker protein, showed increased expression following MBD6 overexpression in hATSCs after induction of differentiation. We also evaluated neural differentiation potency by immunocytochemistry. Neuronal markers (TUJ and NF160) and GFAP expression were markedly higher in cells overexpressing MBD6 than in control cells. Conversely, MBD6-depleted cells showed a considerable decrease in neural differentiation efficiency and neural lineage-related gene expression (Fig. 6g, h). We are also evaluated transdifferentiation potency of MBD6 overexpressing hATSC the in vivo SCID mouse brain. As shown in Fig. 7, MBD6 in hATSCs significantly enhanced neural differentiation potency compared to control hATSCs (Fig. 7). Immunohistochemical analysis revealed that a significantly high percentage of MBD6 hATSCs was differentiated into TuJ+, GABA+, and MAP2ab+ neuronal cells in the SCID mouse brain (Fig. 7). Figure 8 presents the overall global regulation pathway of MBD6/Oct4 for self-renewal and differentiation of hATSCs.

Discussion

We investigated novel signaling pathways involving nuclear Ago2, Oct4, and MBD6 that affect self-renewal and differentiation in cultured hATSCs. We performed ChIP/PCR analysis to identify new Oct4-regulating target genes that would explain how Oct4 maintains its self-renewal capacity and observed that MBD6 gene expression was regulated by Oct4 binding to the promoter region of the MBD6 gene. The MBD protein family includes six members: MBD1 and MBD2 mediate gene binding to methylated DNA and recruit histone deacetylase [20–22, 27, 28], MBD3 does not directly bind to methylated DNA but is a component of NURD complexes, which regulate ATP-dependent nucleoside remodeling [30–32], and MBD4 is involved in DNA repair [33]. The functions of MBD5 and MBD6 have not been fully described. To characterize the function of MBD6, we measured MBD6, Ago2, and Oct4 mRNA expression levels. Consistent with the results of our earlier work, nuclear Ago2 regulated Oct4 gene expression [2, 11]. Thus, we expected a coordinated role of MBD6 on stem cell self-renewal and differentiation potency. We found that MBD6 is a direct target of Oct4, based on the result that MBD6 gene expression was altered after Oct4 bound to the regulatory region of the MBD6 gene. Our previous study showed that MBD6 overexpression significantly improves stem cell behavior in vitro, such as cell proliferation and transdifferentiation into various lineages of mature cells. MBD6 appeared to act as a key regulator of the cell cycle and differentiation in both a positive and reciprocal feedback loop, which is activated by Oct4. According to that result, we found that the differential MBD6 expression level at a specific passage of hATSCs culture was coordinated with the subsequent differential expression of Oct4 at a specific passage of hATSCs (Fig. 4b). Here, we used ChIP-PCR analysis to identify novel MBD6 target genes, which can be classified into three groups: cell-cycle-related genes, MBD family genes, and genes that control stemness. The cell cycle-related genes (BRCA2, USP44, and STAT3) showed increased gene expression by MBD6. The second group was composed of MBD2, MBD3, and MBD4; these genes negatively regulate the cell cycle through negative transcriptional regulation via interactions with methylated genes [34]. MBD2 and MBD3 were incorporated during the S phase of the cell cycle and attenuated cell proliferation. The third group, such as Oct4, Nanog, and REST, was involved in stemness.

We induced differentiation into mesodermal and neural lineages after MBD6 overexpression or depletion. MBD6 overexpression significantly reduced the ability of hATSCs to differentiate into mesodermal lineages, such as bone, fat, and cartilage. In contrast, MBD6 overexpression effectively enhanced neuronal differentiation potency in hATSCs. MBD6-mediated transdifferential potencies were a consequence of the differential expression of Oct4. Oct4 binds to the MBD6 promoter region and positively controls MBD6 expression. Nanog and REST expression levels were also positively regulated by MBD6. We had already determined that MBD6 influenced cell morphology and specific gene expression.

MBD6 function and regulation of gene-related expression has been poorly understood until now. In this study, we found that MBD6 specifically controlled genes for stemness and cell cycle regulators in hATSCs. MBD6 was also influenced by Oct4, implying a reciprocal interaction between the two factors. We also discovered an interaction

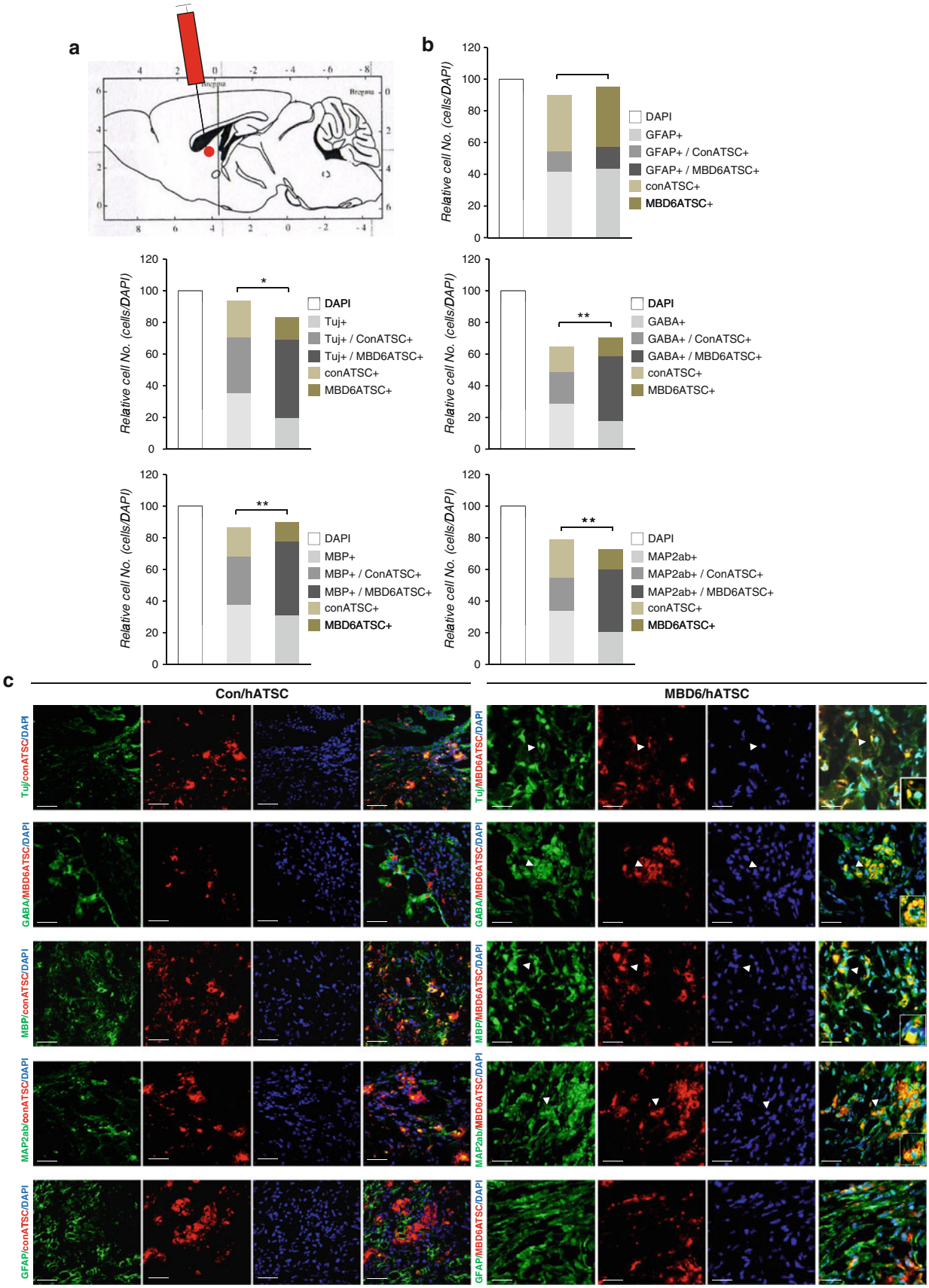
a
b
Relative cell No. (cells/DAPI)
DAPI
GFAP+
GFAP+ / ConATSC+
GFAP+ / MBD6ATSC+
conATSC+
MBD6ATSC+
Tuj+
Tuj+ / ConATSC+
Tuj+ / MBD6ATSC+
GABA+
GABA+ / ConATSC+
GABA+ / MBD6ATSC+
MBP+
MBP+ / ConATSC+
MBP+ / MBD6ATSC+
MAP2ab+
MAP2ab+ / ConATSC+
MAP2ab+ / MBD6ATSC+
c
Con/hATSC
MBD6/hATSC
Tuj/conATSC/DAPI
Tuj/MBD6ATSC/DAPI
GABA/MBD6ATSC/DAPI
MBP/conATSC/DAPI
MBP/MBD6ATSC/DAPI
MAP2ab/conATSC/DAPI
MAP2ab/MBD6ATSC/DAPI
GFAP/conATSC/DAPI
GFAP/MBD6ATSC/DAPI

◀ **Fig. 7** Exogenic MBD6-overexpressing hATSCs effectively induce neuronal differentiation in the in vivo SCID mouse brain. **a** In vivo evaluation of neurogenic activity of MBD6+ hATSCs or control hATSCs. Specific region of SCID mouse brain (striatum) for cell engraftment of hATSCs before and after MBD6 overexpression. **b**, **c** Relative numbers of neural differentiated hATSCs were counted after immunohistochemical staining of SCID mouse brains using anti-Tuj, anti-GABA, anti-MBP, and anti-GFAP antibodies. The transdifferentiation potency of engrafted MBD6+ hATSCs and control hATSCs was determined via immune marked cell counting and a comparison of both tissue samples. To trace engrafted cells in the brain, engrafting cells were marked using CM-Dil

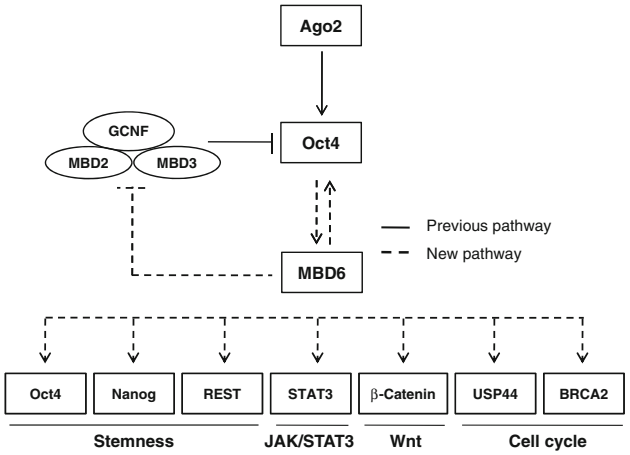

Fig. 8 Global gene expression regulation of Ago2/Oct4/MBD6 during self-renewal and differentiation of hATSCs

between MBD6 and MBD family members, including MBD2, MBD3, MBD4, and MBD6 itself. We hypothesize that Oct4 regulates the cell cycle through its interactions with MBD6. MBD6 and Oct4 also directly regulate USP44 and BRCA2. USP44 is an enzyme that plays a crucial role in the anaphase-promoting complex (APC), which triggers the transition from metaphase to anaphase [35]. BRCA2 is a gene associated with breast cancer that is responsible for DNA repair via its recruitment of RAD51 [36]. Although UPS44 and BRCA2 were not fully investigated in this study, we propose that cell proliferation and self-renewal are partly regulated by USP44 and BRCA2 through their control of the cell cycle. Our experimental results reveal that USP44 and BRCA2 expression was correlated with MBD6 expression. Alternatively, cell cycle regulation by MBD6 may be through interactions with other members of the MBD family. Previous studies demonstrated that in S-phase cells, both MBD2 and MBD3 colocalize with DNMT1, a protein that interacts with the cell proliferation marker PCNA [34]. MBD6 has been shown to contain a putative methyl-binding domain that did not bind to methylated DNA, in contrast to other members of the MBD family [37].

In this study, we found that MBD6 directly regulated MBD2 and MBD3, suggesting that MBD6 function was not specific to its putative methyl-binding domain. We hypothesize that MBD6 is a critical master regulator of MBD family members. Based on our ChIP analysis, the majority of MBD family members, except MBD1 and MBD5, were controlled by MBD6. MBD6 function influenced DNA methylation directly or indirectly by the regulation of MBD2 and MBD3. If MBD6 controls MBD2 and MBD3, methylation states should also be changed. Therefore, we performed bisulfate conversion tests and sequencing of the Oct4 gene. We observed approximately 20–30 % demethylation in MBD6-overexpressing cells compared with untreated control cells. To validate our results, we evaluated the relative expression of monomethylated Lys 4 of histone 3 (H3K4me1), bi-methylated Lys 4 of histone 3 (H3K4me2), tri-methylated Lys 4 of histone 3 (H3K4me3), and tri-methylated Lys 27 of histone 3 (H3K27me3) before and after MBD6 interference or overexpression in hATSCs. Consistent with the results outlined above, MBD6 overexpression induced upregulation, and MBD6 knockdown resulted in downregulation of methylation marker gene expression when compared to control cells.

Acknowledgments This work was supported by the National Research Foundation of Korea (NRF) grant funded by the Korea Government (MEST, 2010-0020265).

Conflict of interest None.

References

1. Murchison EP, Partridge JF, Tam OH, Cheloufi S, Hannon GJ (2005) Characterization of Dicer-deficient murine embryonic stem cells. Proc Natl Acad Sci USA 102:12135–12140
2. Jang JH, Jung JS, Im YB, Kang KS, Choi JI, Kang SK (2012) Crucial role of nuclear Ago2 for hUCB-MSCs differentiation and self-renewal via stemness control. Antioxid Redox Signal 16:95–111
3. Tan GS, Garchow BG, Liu X, Yeung J, Morris JPt, Cuellar TL, McManus MT, Kiriakidou M (2009) Expanded RNA-binding activities of mammalian Argonaute 2. Nucleic Acids Res 37: 7533–7545
4. Farh KK, Grimson A, Jan C, Lewis BP, Johnston WK, Lim LP, Burge CB, Bartel DP (2005) The widespread impact of mammalian MicroRNAs on mRNA repression and evolution. Science 310:1817–1821
5. Norddahl GL, Pronk CJ, Wahlestedt M, Sten G, Nygren JM, Ugale A, Sigvardsson M, Bryder D (2011) Accumulating mitochondrial DNA mutations drive premature hematopoietic aging phenotypes distinct from physiological stem cell aging. Cell Stem Cell 8:499–510
6. Chambers I, Smith A (2004) Self-renewal of teratocarcinoma and embryonic stem cells. Oncogene 23:7150–7160
7. Kang SK, Lee DH, Bae YC, Kim HK, Baik SY, Jung JS (2003) Improvement of neurological deficits by intracerebral

transplantation of human adipose tissue-derived stromal cells after cerebral ischemia in rats. Exp Neurol 183:355–366
8. Kelly DP (2011) Cell biology: ageing theories unified. Nature 470:342–343
9. Kim JH, Lee MR, Jee MK, Kang SK (2008) Selenium induces improvement of stem cell behaviors in human adipose-tissue stromal cells via SAPK/JNK and stemness acting signals. Stem Cells 26:2724–2734
10. Mattson MP (2011) A reaction to mitochondria in action. Cell Res 21:279–282
11. Kim BS, Jung JS, Jang JH, Kang KS, Kang SK (2011) Nuclear Argonaute 2 regulates adipose tissue-derived stem cell survival through direct control of miR10b and selenoprotein N1 expression. Aging Cell 10:277–291
12. Meister G, Landthaler M, Patkaniowska A, Dorsett Y, Teng G, Tuschl T (2004) Human Argonaute2 mediates RNA cleavage targeted by miRNAs and siRNAs. Mol Cell 15:185–197
13. Takahashi K, Yamanaka S (2006) Induction of pluripotent stem cells from mouse embryonic and adult fibroblast cultures by defined factors. Cell 126:663–676
14. Yamanaka S, Takahashi K (2006) Induction of pluripotent stem cells from mouse fibroblast cultures. Tanpakushitsu Kakusan Koso 51:2346–2351
15. Davey C, Pennings S, Allan J (1997) CpG methylation remodels chromatin structure in vitro. J Mol Biol 267:276–288
16. Kass SU, Pruss D, Wolffe AP (1997) How does DNA methylation repress transcription? Trends Genet 13:444–449
17. Ng HH, Bird A (1999) DNA methylation and chromatin modification. Curr Opin Genet Dev 9:158–163
18. Razin A (1998) CpG methylation, chromatin structure and gene silencing-a three-way connection. EMBO J 17:4905–4908
19. Meehan RR, Lewis JD, McKay S, Kleiner EL, Bird AP (1989) Identification of a mammalian protein that binds specifically to DNA containing methylated CpGs. Cell 58:499–507
20. Jones PL, Veenstra GJ, Wade PA, Vermaak D, Kass SU, Landsberger N, Strouboulis J, Wolffe AP (1998) Methylated DNA and MeCP2 recruit histone deacetylase to repress transcription. Nat Genet 19:187–191
21. Nan X, Ng HH, Johnson CA, Laherty CD, Turner BM, Eisenman RN, Bird A (1998) Transcriptional repression by the methyl-CpG-binding protein MeCP2 involves a histone deacetylase complex. Nature 393:386–389
22. Ng HH, Zhang Y, Hendrich B, Johnson CA, Turner BM, Erdjument-Bromage H, Tempst P, Reinberg D, Bird A (1999) MBD2 is a transcriptional repressor belonging to the MeCP1 histone deacetylase complex. Nat Genet 23:58–61
23. Cross SH, Meehan RR, Nan X, Bird A (1997) A component of the transcriptional repressor MeCP1 shares a motif with DNA methyltransferase and HRX proteins. Nat Genet 16:256–259
24. Hendrich B, Bird A (1998) Identification and characterization of a family of mammalian methyl-CpG binding proteins. Mol Cell Biol 18:6538–6547
25. Ohki I, Shimotake N, Fujita N, Nakao M, Shirakawa M (1999) Solution structure of the methyl-CpG-binding domain of the methylation-dependent transcriptional repressor MBD1. EMBO J 18:6653–6661
26. Wakefield RI, Smith BO, Nan X, Free A, Soteriou A, Uhrin D, Bird AP, Barlow PN (1999) The solution structure of the domain from MeCP2 that binds to methylated DNA. J Mol Biol 291:1055–1065
27. Wade PA, Gegonne A, Jones PL, Ballestar E, Aubry F, Wolffe AP (1999) Mi-2 complex couples DNA methylation to chromatin remodelling and histone deacetylation. Nat Genet 23:62–66
28. Zhang Y, Ng HH, Erdjument-Bromage H, Tempst P, Bird A, Reinberg D (1999) Analysis of the NuRD subunits reveals a histone deacetylase core complex and a connection with DNA methylation. Genes Dev 13:1924–1935
29. Jang JH, Jung JS, Choi JI, Kang SK (2012) Nuclear Ago2/HSP60 contributes to broad spectrum of hATSCs function via Oct4 regulation. Antioxid Redox Signal 16(5):383–399
30. Jiang CL, Jin SG, Pfeifer GP (2004) MBD3L1 is a transcriptional repressor that interacts with methyl-CpG-binding protein 2 (MBD2) and components of the NuRD complex. J Biol Chem 279:52456–52464
31. Sakai H, Urano T, Ookata K, Kim MH, Hirai Y, Saito M, Nojima Y, Ishikawa F (2002) MBD3 and HDAC1, two components of the NuRD complex, are localized at Aurora-A-positive centrosomes in M phase. J Biol Chem 277:48714–48723
32. Zhu D, Fang J, Li Y, Zhang J (2009) Mbd3, a component of NuRD/Mi-2 complex, helps maintain pluripotency of mouse embryonic stem cells by repressing trophectoderm differentiation. PLoS ONE 4:e7684
33. Petronzelli F, Riccio A, Markham GD, Seeholzer SH, Stoerker J, Genuardi M, Yeung AT, Matsumoto Y, Bellacosa A (2000) Biphasic kinetics of the human DNA repair protein MED1 (MBD4), a mismatch-specific DNA N-glycosylase. J Biol Chem 275:32422–32429
34. Tatematsu KI, Yamazaki T, Ishikawa F (2000) MBD2–MBD3 complex binds to hemi-methylated DNA and forms a complex containing DNMT1 at the replication foci in late S phase. Genes Cells 5:677–688
35. Zhang Y, van Deursen J, Galardy PJ (2011) Overexpression of ubiquitin specific protease 44 (USP44) induces chromosomal instability and is frequently observed in human T-cell leukemia. PLoS ONE 6:e23389
36. Badie S, Escandell JM, Bouwman P, Carlos AR, Thanasoula M, Gallardo MM, Suram A, Jaco I, Benitez J, Herbig U, Blasco MA, Jonkers J, Tarsounas M (2010) BRCA2 acts as a RAD51 loader to facilitate telomere replication and capping. Nat Struct Mol Biol 17:1461–1469
37. Laget S, Joulie M, Le Masson F, Sasai N, Christians E, Pradhan S, Roberts RJ, Defossez PA (2010) The human proteins MBD5 and MBD6 associate with heterochromatin but they do not bind methylated DNA. PLoS ONE 5:e11982